Iraqi Journal of Physics, 2019 *Vol.17, No.40, PP. 77-87*
DOI: 10.20723/ijp.17.40.77-87

Synthesized pure cobalt oxide nanostructure and doped with yttrium by hydrothermal method for photodetector applications

Suhad A. Hamdan and Iftikhar M. Ali

Department of Physics, College of Science, University of Baghdad

E-mail: suhadah22@gmail.com

Abstract

In this study, pure Co_3O_4 nano structure and doping with 4 %, and 6 % of Yttrium is successfully synthesized by hydrothermal method. The XRD examination, optical, electrical and photo sensing properties have been studied for pure and doped Co_3O_4 thin films. The X-ray diffraction (XRD) analysis shows that all films are polycrystalline in nature, having cubic structure.

The optical properties indication that the optical energy gap follows allowed direct electronic transition calculated using Tauc equation and it increases for doped Co_3O_4. The photo sensing properties of thin films are studied as a function of time at different wavelengths to find the sensitivity for these lights.

High photo sensitivity doped Co_3O_4 with 6% of Yttrium, is a 118.774% at wavelength 620 nm, while for pure Co_3O_4 films no sensitivity at the same wavelength. So, higher sensitivity is found for doping Co_3O_4 with fast rise and fall times less than 1s.

Key words

Cobalt oxide, yttrium, photo sensor, sensitivity, hydrothermal.

Article info.

Received: Sep. 2018
Accepted: Nov. 2018
Published: Mar. 2019

تحضير اوكسيد الكوبلت النانوية والمطعمة بالايتريوم المحضرة بطريقة الهيدروثرميل لتطبيقات الكاشف الضوئي

سهاد عبد الكريم حمدان و افتخار محمود علي

قسم الفيزياء، كلية العلوم، جامعة بغداد

الخلاصة

في هذا العمل تم تحضير Co_3O_4 النانوية التركيب النقية والمطعمة ب 4٪ و 6 ٪ يتتريوم بنجاح بطريقة الهيدروثرمل. تحليل الاشعة السينية والخصائص البصرية والخصائص الكهربائية وخصائص استشعار الضوء درست للاغشية المحضرة من Co_3O_4 النقي والمطعم بالايتريوم. اظهر تحليل الاشعة السينية كل الاغشية المحضرة متعددة التبلور في طبيعتها وتمتلك تركيب مكعب.

تبين الخواص البصرية أن فجوة الطاقة الضوئية تتبع الانتقال الإلكتروني المباشر المحسوب باستخدام معادلة تاوس وتزداد مع تطعيم Co_3O_4. خصائص تحسسية الضوء للاغشية تم تحقق منها كدالة للزمن عند اطوال موجية مختلفة لايجاد التحسسية لهذه الاضواء.

حساسية عالية للضوء عند تطعيم Co_3O_4 مع 6 ٪ من الإيتريوم، هي 118.774 ٪ عند الطول الموجي 620 نانومتر، في حين أنه لا توجد حساسية لافلام Co_3O_4 النقية عند نفس الطول الموجي. لذلك، يتم الحصول على حساسية أعلى لـ Co_3O_4 المطعم مع أوقات الصعود والهبوط السريع أقل من 1 ثانية.

Introduction

Cobalt oxide (Co_3O_4) is an important P-type semiconductor with direct optical band gaps at 1.48 and 2.19 eV [1, 2]. Co_3O_4 has been used as a gas sensor and catalyst in hydrocracking processes of crude fuels, pigment for glasses and ceramic [3, 4]. Hydrothermal synthesis can be defined as a technique that be determined by the solubility of minerals in hot environment under high pressure to get interested nanostructure where the crystal growth

is achieved in an instrument consisting of a steel pressure vessel named an autoclave [5]. Electrical conductivity subsequent of photo-induced electron excitations in which light are absorbed is called Photoconductivity (PC). In semiconductors, photoconductivity rises due to interaction of photons with bound electrons of lattice atoms that leads to photo-generation of electron-hole pairs when absorption of photons which increases carrier density and conductivity of material [6]. PC is an essential tool to study the properties of semiconducting materials such as the nature of photo-excitation and recombination processes. The conductivity of material depends upon the carrier lifetime, carrier density and complex process of carrier generation, recombination, and trapping [7]. It is also a function of temperature, intensity of light, applied field, and energy of radiation [8].

This research goals to prepare pure cobalt oxide nanoparticle and doped it with Yttrium and study their structural, morphological, optical properties and its application as a photodetector device.

Experimental

Pure Cobalt Oxide and doped with yttrium Oxide thin films have been syntheses using hydrothermal method onto seeded layer. Initially, to prepare seeded layer, PVA $(C_4H_6O_2)_n$ will be used which dissolved in distilled water. The aqueous solutions of cobalt nitrate and Yttrium nitrate with 0.1M are stirred separately on magnetic stirrer for 10 min to prepare the precursors which are the sources of cobalt and yttrium ions. Then, cobalt precursor is additional to 1.5 g of PVA at 80 ^oC for 2 h. This solution is irradiated with 2.4 GHz microwave frequency at power 220 W for 10 min then determining pH for solution and controlled its value to 8 or until changing the color of solution. The resultant solution has been spin coated onto silicon and glass substrates at 1500 rpm for 1min, this step was repeated a number of times to get the desired thickness for seed layer.

The above steps are for preparation of pure seed layer solution, for preparing seed layer solution with Yttrium, the identical steps have been done but mixing the two salts which are cobalt nitrate and yttrium nitrate on magnetic stirrer for 1 h at 70 ^oC before adding PVA solution. Lastly, these seed layers have been dried at 120 ^oC for a few minutes so as to get suitable adhesion of the seeded particles on the surface of the substrate. The chief purpose of using seed layer is to supply nucleation sites by diluting the thermodynamic barrier between heterogeneous materials and when seed layer was used, the grown nanostructures were create to be highly dense, well aligned and uniform [9]. These seeded layers are thermal annealed at 210 ^oC for 1 h to vanish PVA, then annealed at 380 ^oC for 2 hour to improve crystallinity and remove hydroxide phase, now samples are being standing by to the following step which is growth process. To prepare growth solution, 0.1 M cobalt nitrite (as a source of cobalt ions) and 0.1 M Hexamine $C_6H_{12}N_4$ (as oxidized agent) are dissolved separately in distilled water and stirred for 10 min. Then, these two solutions are mixed and stirred for 10 min. For cobalt oxide doped with yttrium oxide preparation, the identical procedure is done but before addition hexamine, yttrium nitrate (as a source of yttrium ions) is added to cobalt nitrate with suitable amount and stirred together at 70 ^oC for 1h to permit these two elements to well disperse, after 1 h hexamine is added. The mixture was transferred into a Teflon-lined stainless steel autoclave where the substrates with seeded layers are vertically aligned

inside the Teflon container. The autoclave was closed speedily and preserved at 100 ^{o}C for 4h in a digital temperature controlled oven. Then, the autoclave was cooled to room temperature naturally. The substrates are washed with distilled water to eliminate any residual solid particles from the surface or unreacted atoms, then the samples are dried in oven at 100^{o}C for 30 min. Annealing process will be done inside furnace at 500 ^{o}C for 1h to convert hydroxide phase $Co(OH)_2$ into Co_3O_4. After that, the films are ready to be characterized.

The structural properties are determined by X-ray diffraction (XRD- 6000 Labx, supplied by Shimadzu, X-ray source is Cu). The optical absorption spectra were found using UV–VIS spectrophotometer "OPTIMA SP-3000" within the wavelength range of (190-1100) nm.

Results and discussion

1- Structural properties (XRD)

X-ray diffraction patterns of prepared pure and doped cobalt oxide grown onto p-type silicon substrates are revealed in Fig.1. It can be observed that the patterns show diffraction peaks about (2θ~ 31.5044^{o}, 37.0796^{o}, 38.8496^{o}, 44.9558^{o}, 56.0177^{o}, 59.6460^{o} and 65.3097^{o}) denoted to (202), (311), (222), (400), (422), (333) and (404) preferred directions respectively for cobalt oxide which is in agreement with (ASTM) card number 96-900-5888.

In addition to these peaks it can be observed that the patterns exhibit diffraction peaks about (2θ~ 33.8230^{o}, 48.7611^{o} and 57.8200^{o}) denoted to (400), (440) and (622) preferred directions respectively for yttrium oxide as revealed in Table 1, which is in agreement with (ASTM) card number 96-100-9018 which shows the cubic structure and identical peaks appeared with the researchers [10-12]. Crystallite size is estimated by Scherer's formula equation [12]:

$$D = \frac{K\lambda}{\beta cos\theta} \quad (1)$$

where K is the shape factor (0.94), λ is 0.15405 nm which is the wavelength of the x-ray source, β is the full width at half-maximum (FWHM) and θ is the angle of the diffraction peak [10]. The average crystallite size D is 12.6 nm for pure cobalt oxide and it is decreasing with doping reach it to 12.3 nm at doping with 6 % Yttrium. Lattice constant a is calculated by using the predominated orientation (311) from the next equation [10]:

$$d_{hkl} = \frac{a}{\sqrt{h^2 + k^2 + l^2}} \quad (2)$$

where hkl are miller indices and d_{hkl} is interplaner spacing which is calculated using Bragg law

$$n\lambda = 2\, d_{hkl} \sin\theta \quad (3)$$

The calculated lattice constant of cobalt oxide nanostructure grown on silicon was 8.0348 Å and it was the minimum value 8.0109 Å for cobalt oxide nanostructure doping with 2% Yttrium. Strain is calculated by the following relations [13, 14]:

$$s = \frac{a - a_o}{a_o} x100\% \quad (4)$$

where a_o is the standard lattice constant for unstained cobalt oxide lattice which equals 8.084Å. The values of strain are -0.00609, -0.00846 and -0.00793 for pure cobalt oxide and doping with 4 %, and 6 % with yttrium respectively. The negative value for strain is associated to the compressive strain which is due to the nanosize effect, as revealed in Table 2. Table 1 shows structural parameters calculated from XRD spectra for cobalt oxide and cobalt yttrium oxide. The adding of yttrium causes deformation or distortion to Co_3O_4 lattice, this may be due to large ionic radius of Y^{+3} which equals 0.9 Å compared with that of Co^{+3} which is 0.63 Å [15].

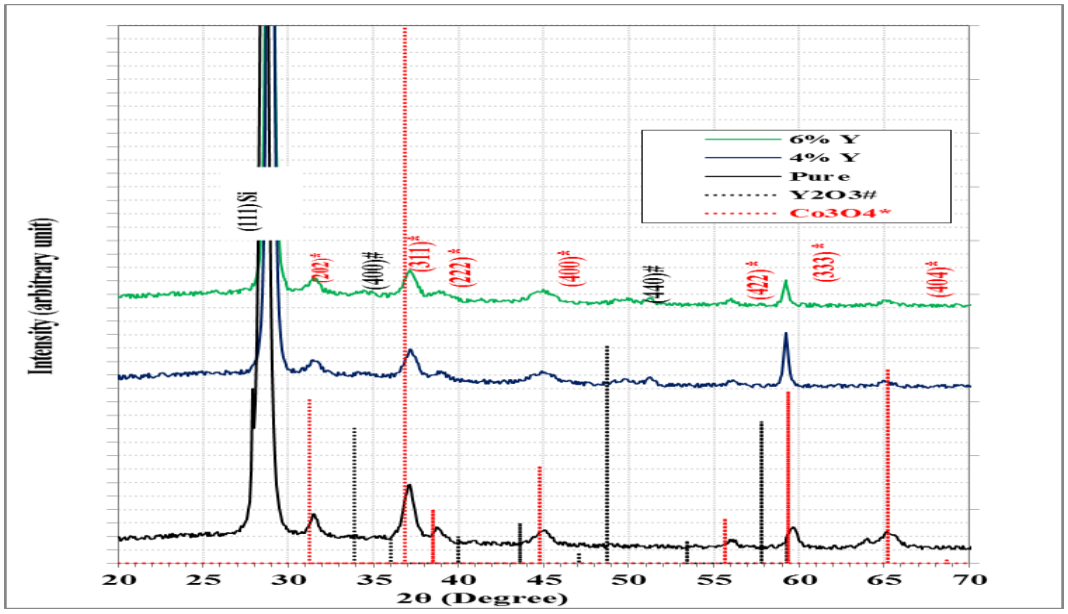

Fig. 1: XRD patterns of cobalt oxide and cobalt yttrium oxide grown onto Si p-type substrates

Table 1: Structure Parameters for Co_3O_4 and cobalt yttrium oxide.

Y%	2θ (Deg.)	β (FWHM (Deg.)	d_{hkl} Exp.(Å)	G.S (nm)	hkl	d_{hkl} Std.(Å)	Phase	Card No.
0	31.5044	0.4779	2.8374	17.3	(202)	2.8589	Co_3O_4	96-900-5888
	37.0796	0.7168	2.4226	11.7	(311)	2.4375	Co_3O_4	96-900-5888
	38.8496	0.6371	2.3162	13.2	(222)	2.3349	Co_3O_4	96-900-5888
	44.9558	1.0354	2.0148	8.3	(400)	2.0219	Co_3O_4	96-900-5888
	56.0177	0.6372	1.6403	14.1	(422)	1.6498	Co_3O_4	96-900-5888
	59.6460	0.6372	1.5489	14.4	(333)	1.5550	Co_3O_4	96-900-5888
	65.3097	1.0354	1.4276	9.1	(404)	1.4286	Co_3O_4	96-900-5888
4	31.5000	0.8081	2.8378	10.2	(202)	2.8589	Co_3O_4	96-900-5888
	37.1721	0.8081	2.4168	10.4	(311)	2.4375	Co_3O_4	96-900-5888
	38.9446	0.8980	2.3108	9.4	(222)	2.3349	Co_3O_4	96-900-5888
	44.9712	1.5266	2.0141	5.6	(400)	2.0219	Co_3O_4	96-900-5888
	56.0495	0.6286	1.6394	14.3	(422)	1.6498	Co_3O_4	96-900-5888
	59.2400	0.3592	1.5585	25.5	(333)	1.5550	Co_3O_4	96-900-5888
	65.0900	0.8082	1.4319	11.7	(404)	1.4286	Co_3O_4	96-900-5888
6	31.4786	0.8188	2.8397	10.1	(202)	2.8589	Co_3O_4	96-900-5888
	34.5805	**1.1827**	**2.5917**	**7.0**	**(400)**	**2.6434**	**Y_2O_3**	**96-100-9018**
	37.1507	0.8188	2.4181	10.2	(311)	2.4375	Co_3O_4	96-900-5888
	38.9232	0.9099	2.3120	9.3	(222)	2.3349	Co_3O_4	96-900-5888
	44.9498	1.5467	2.0150	5.6	(400)	2.0219	Co_3O_4	96-900-5888
	49.7356	**1.2737**	**1.8318**	**6.9**	**(440)**	**1.8681**	**Y_2O_3**	**96-100-9018**
	56.0281	0.6369	1.6400	14.1	(422)	1.6498	Co_3O_4	96-900-5888
	59.2186	0.3639	1.5590	25.1	(333)	1.5550	Co_3O_4	96-900-5888
	65.1200	0.8189	1.4313	11.5	(404)	1.4286	Co_3O_4	96-900-5888

Table 2: Lattice constant, strain and Crystallite size for pure Co_3O_4 films and doped with Y.

Doping ratio %	$a_{exp.}$	$a_{std.}$	strain(S)= $a_{std.}-a_{exp.}/a_{std.}$	Average Crystallite size (D_{ave})(nm)
0	8.0348	8.084	-0.00609	12.6
4	8.0156		-0.00846	12.4
6	8.0199		-0.00793	12.3

2- Optical properties

UV visible absorbance spectra of pure Co_3O_4 and doped with yttrium oxide thin films in the range (200-1100) nm has been examined as in Fig.2. The shoulder or peak position reflects the band gap of the nanoparticles, the peak of the spectra corresponds to the fundamental absorption edges in the sample [16]. It can be showed two regions of optical transitions which is in agreement with Shinde et al. [17]. As well, there is blue shift in absorption edges toward low wavelengths with yttrium adding which it may be associated to the size decreasing of particles and attributed to the quantum confinement of nanoparticles. Moreover, the absorbance intensity decreases which may be due to the distortion in the crystal structure.

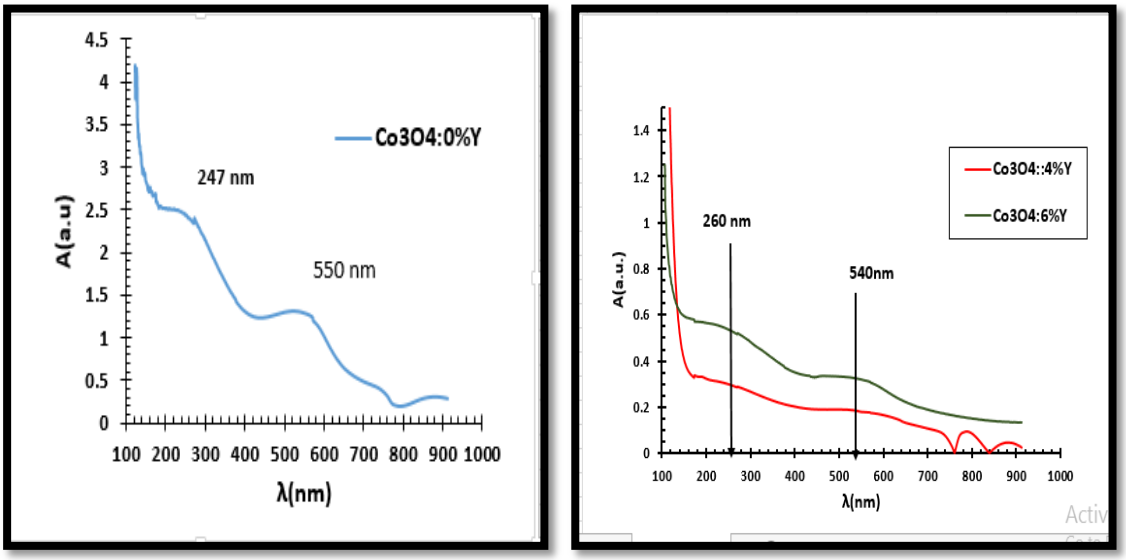

(a) (b)

Fig.2: UV-Vis absorption spectra of (a) Co_3O_4 and (b) Co_3O_4 doping with 0.04, and 0.06 yttrium oxide.

To evaluate the value of the direct band gap from the above absorption spectra one can use Tauc relation [18]:

$$(\alpha h\nu)^n = B(h\nu - E_g) \quad (5)$$

where $h\nu$ is the photon energy in eV, α is the absorption coefficient in cm^{-1}, B is a constant connected to the material, while the value of n is 2 for direct transitions, as in Co_3O_4 has a direct allowed band gap as shown via [1,2, 15]. The band gap energy is found by extrapolating the linear part of the $(\alpha h\nu)^2$ verses photon energy ($h\nu$) on the axis $(\alpha h\nu)^2=0$ as revealed in Fig.3.

The optical absorption studies demonstration that there are two direct band gaps in Co_3O_4, the chief energy band gap and a sub-band located inside the main energy gap, the values of these energy band gaps were determined to be 2.65 and 1.9 eV, respectively, which suffer from blue shift with respect to bulk Co_3O_4. The corresponding values for the band gaps

in the bulk are stated to be 2.13 and 1.52 eV [19]. The observed blue shift in the band gap was explained as originating in the finite size effects of the nanoparticles. For energy gap of doping cobalt oxide with Yttrium, blue shift happened, i.e. the optical energy gap increases with respect to Co_3O_4 with doping with Yttrim, this an indication that a strong quantum confinement happened and the particle size decreased, Table 3 revealed the results of energy gap for pure and doped Co_3O_4.

Two direct optical band gaps are observed in Co_3O_4 attributed to the excitations emanating from the existence of Co in two valence states +2 and +3 respectively. The Co^{3+} *d* states form a small sub-band within the chief band gap while the Co^{2+} *d* states lie nearly at the edge of the conduction band, while the valence band has a primarily O 2*p* character [20].

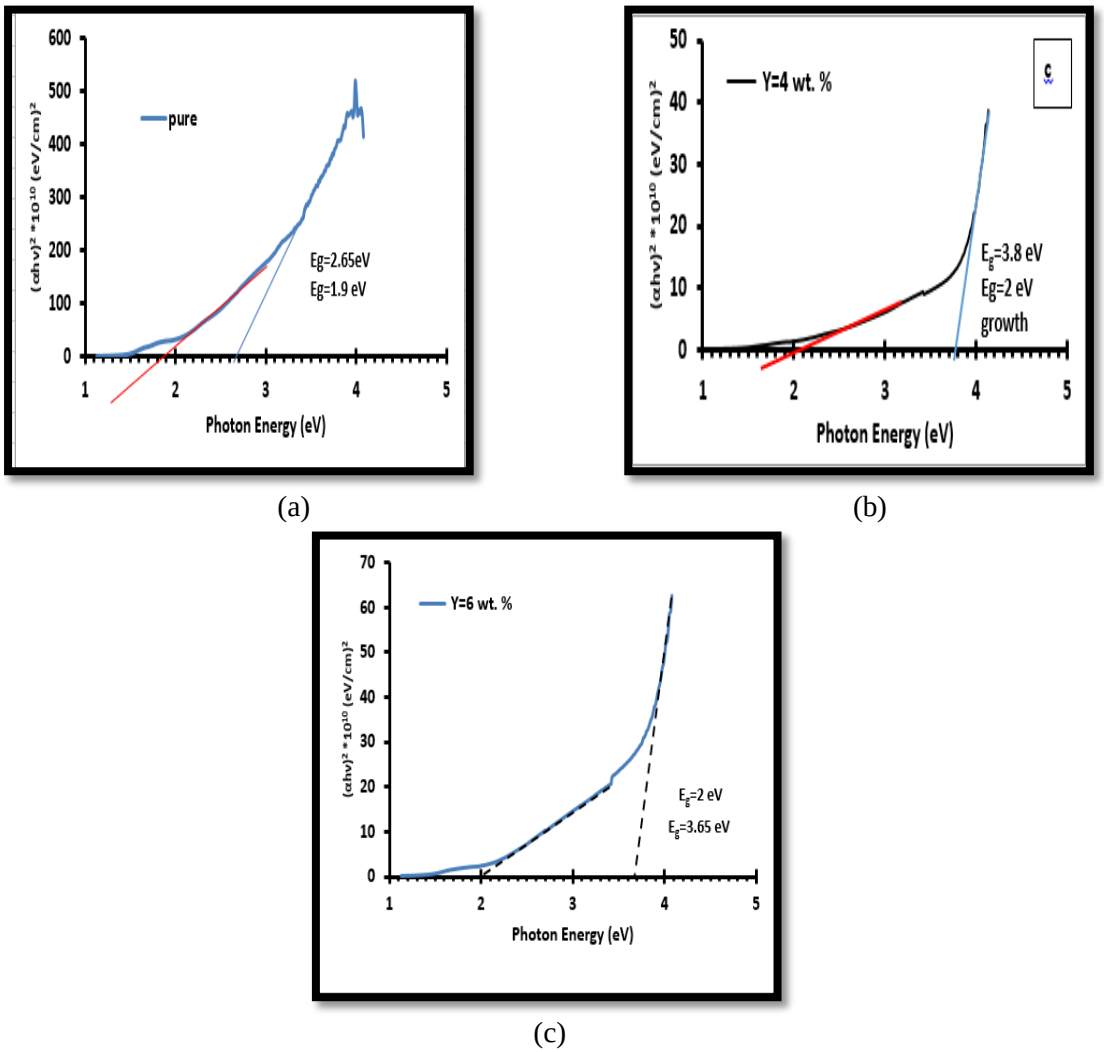

Fig.3: Tauc plot of (a) pure Co_3O_4, (b) doped Co_3O_4 with 4 % yttrim and (c) doped Co_3O_4 with 6 % yttrim.

Table 3: Energy gap estimated from Tauc relation of pure and doped Co_3O_4 with Y.

Y%	Eg1	Eg2
0	1.9	2.65
4	2	3.8
6	2	3.65

3- Current -Voltage (I-V) characteristics

I-V curve of photoconductive detector was measured in dark and under illumination. Fig.4 illustrated the characteristic current–voltage properties of pure Co_3O_4 and doped with Yttrium nanostructures, respectively. The measurement has been done under light with changing the intensities and the photocurrent increases with increasing light intensity. The measurements have been done with sweep voltage from -1V to 1V.

The forward dark current is due to the flow of majority carriers and the applied voltage injects majority carriers which cause the decreasing of the built-in potential, in addition to the width of the depletion layer. As the majority and minority carrier concentration is higher than the intrinsic carrier concentration (n^2_i < np) which produce the recombination current at the low voltage region (0-0.35) Volt. This is due to the excitation of electrons from valence band (V.B) to conduction band (C.B) will recombine with the holes which are found at the V.B., and this is observed by the little increase in recombination current at low voltage region.

Next that there is a fast exponential increase in the current magnitude with increasing of the voltage and this is named diffusion current, which dominates [21]. Whereas the value of the reverse bias current decreases with yttrium addition which is attributed to evolving defects and dislocations that have an influence on the mobility of charge carriers. Besides these defects evolutions allow energy levels to be within the energy gap, these defects may act as active recombination centers, and as a result they decrease current flow across the junction. Fig.4(a) proves the Schottky behavior of the junction for pure and doped Co_3O_4.

4- Responsivity R_λ

Spectral Responsivity R_λ is a performance parameter, definite as the photocurrent generated per unit of power of the incident light intensity on effective areas. The magnitude of the electrical signal output from a photoconductive detector is in response to a specific light power. The responsivity of a photoconductive detector is commonly stated in units of either amperes per watt or volts per watt of incident radiation power. To calculate the spectral responsivity of the tested detector (i.e., the responsivity as a function of wavelength), the photocurrent density produced from the tested detector is simply divided by the calculated power density as in the following equation [22]:

$$R_{\boldsymbol{\lambda}} = J_{ph}(\lambda) / P_{\mathbf{in}}(\boldsymbol{\lambda}) \quad (6)$$

where J_{ph} (λ) is the photocurrent density from the tested detector and P_{in} (λ) is the incident power density measured with the photoconductive detectors as a function of wavelength. Fig.5 shows the responsivity R_λ of pure Co_3O_4 and doped with Y, the responsivity was high in visible region.

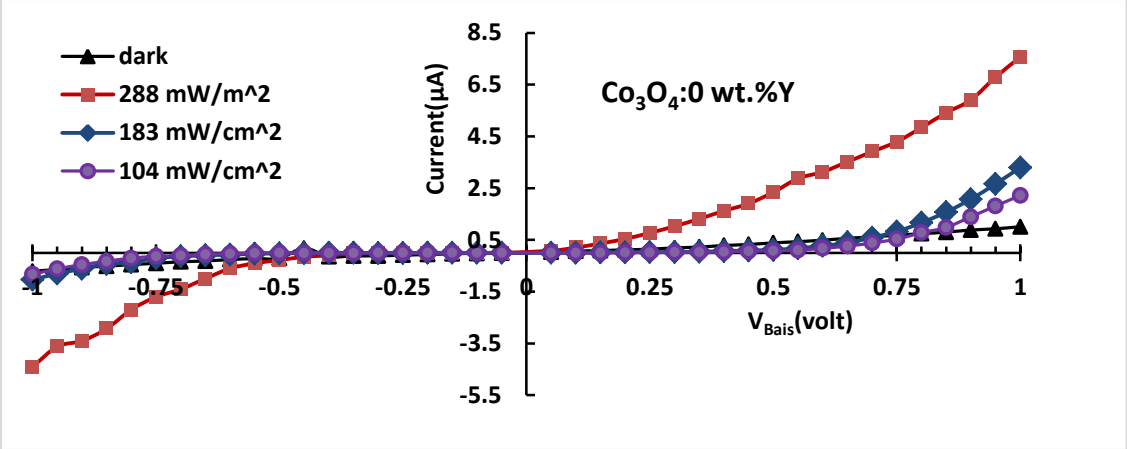

(a)

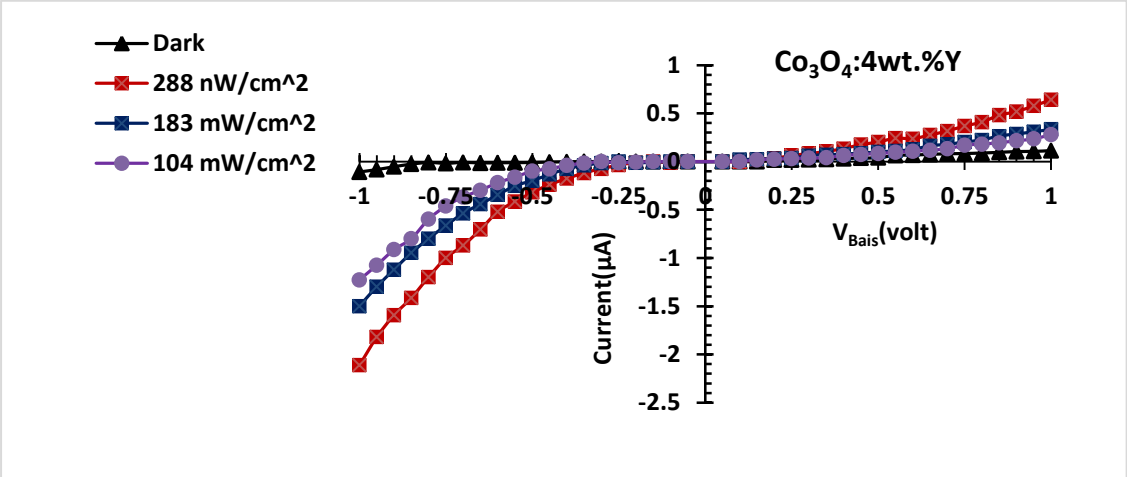

(b)

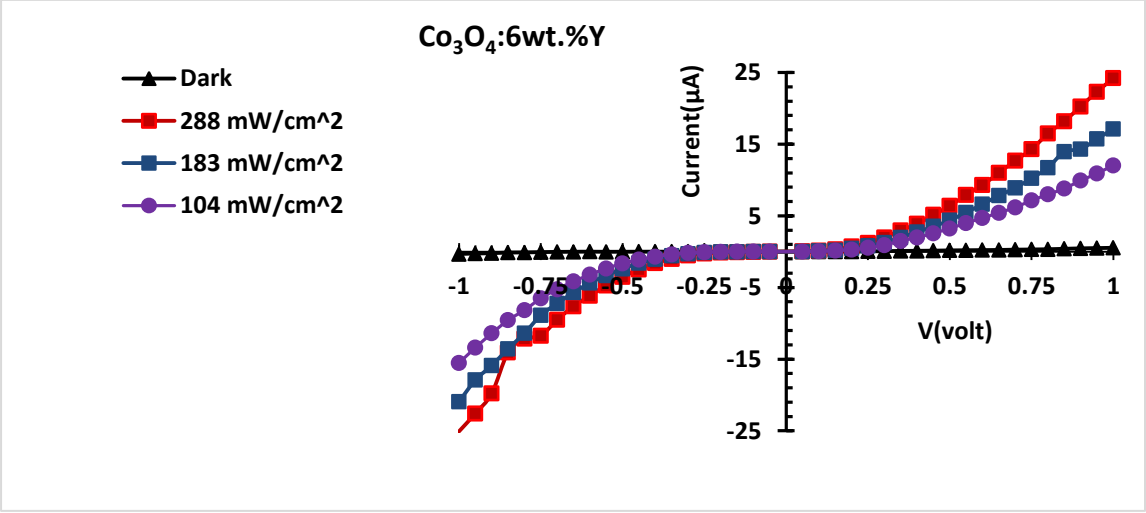

(c)

Fig. 4: I-V characteristics in the dark and under illumination for pure and doped Co_3O_4 with yttrim.

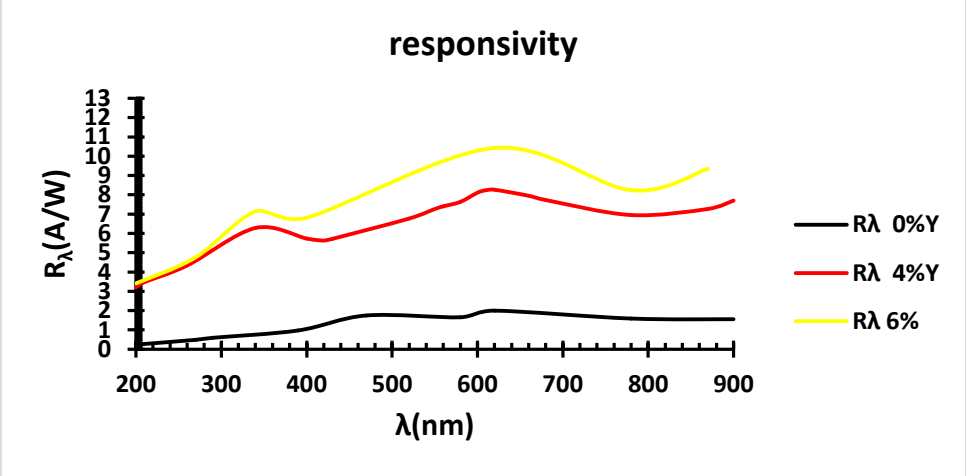

Fig. 5: The variation of spectral responsivity R_λ of undoped and doped Co_3O_4 with yttrium.

5- Photo sensitivity

Conductivity increases after the light is turned on, and after the light is turned off, the current comeback to its original value. This procedure is repeated several time as revealed in Figs.6-8, and the rise time and fall time in this procedure are less than one second for each state turn (ON, OFF). The resistance-time (R-t) characteristics are taken with wavelengths (340, 470, and 620) nm corresponding to maximum responsivity revealed in obvious Fig. 5. Moreover Table 4 demonstrations the sensitivity for pure and doped Co_3O_4 with Yttrium.

From results, the sensitivity increases with yttrium addition and this is attributed to the energy levels presented by the addition atoms lying in the corresponding band gap of Co_3O_4. Such states served as "hopping" states and increased the excitation probability of an electron to the conduction band. So, it becomes clear to be possible to control the response of the current in a semiconducting photodetector due to the electrons in the nanoparticles receive their excitation energy from the power of the light source, it is possible to "switch" these nanoparticles reversibly between higher and lower states of conductivity. The results have been tabulated in Table 4.

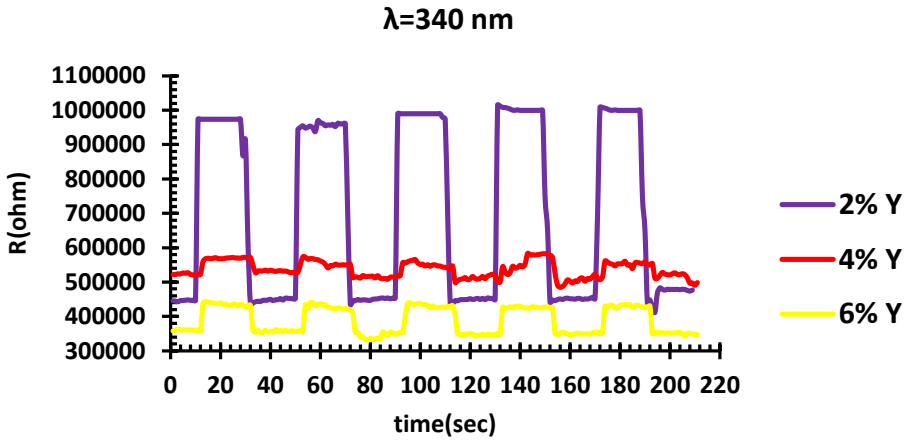

Fig. 6: Photo response time of the prepared undoped and doped Co_3O_4 with yttrium Photo sensor upon exposure to 340 nm light.

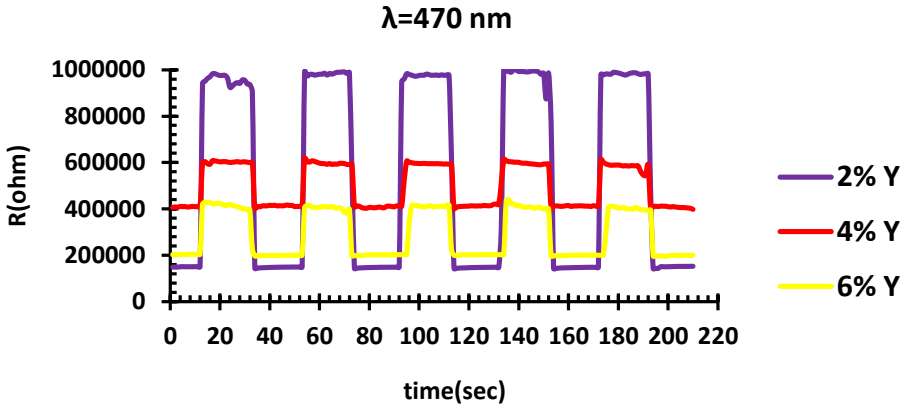

Fig. 7: Photo response time of the prepared undoped and doped Co_3O_4 with yttrium photo sensor upon exposure to 470 nm light.

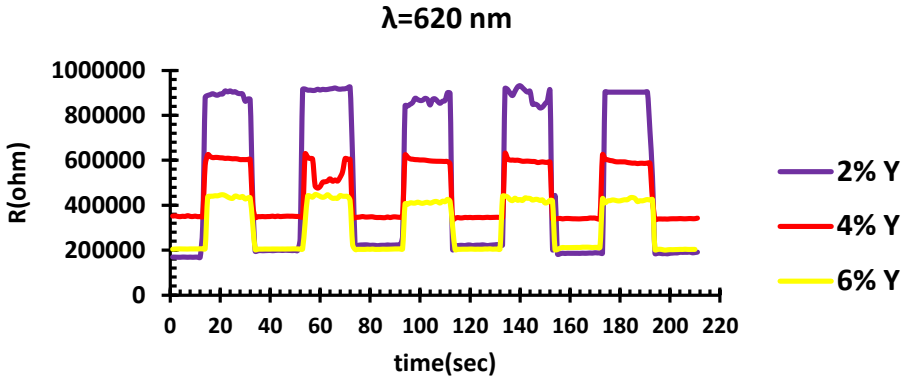

Fig. 8: Photo response time of the prepared undoped and doped Co_3O_4 with yttrium Photo sensor upon exposure to 620 nm light.

Table 4: Photo sensitivity as a function of wavelength for Co_3O_4 :Y/p-Si.

Y%	340 nm	470nm	620 nm
0	-	--	-
4	6.943	45.906	74.527
6	22.661	108.986	118.774

Conclusions

Undoped Co_3O_4 and doped with Yttrium nanostructures were successfully syntheses by hydrothermal technique. Optical energy gap is direct allowed. Photo conductive detector has been successfully fabricated from the syntheses nanostructure. The wavelengths which are near the two energy gaps have been used to examine our devices, higher sensitivity ~ 118.774% at 620 nm and very fast response time < 1sec for Co_3O_4 doping with 6 % Yttrium without any bias voltage, making them having possible applications as electrical gating for binary switching without necessary electric powder.

References

[1] V. Patil, P. Joshi, M. Chougule, S. Sen, Soft Nanoscience Letters, 2 (2012) 1-7.

[2] S. M. Jogade, D. S.Sutrave, V.B.Patil, Int. Journal of Engineering Research and Application, 6, 9 (Part - 4) (2016) 41-46.

[3] L. Estepa, M. Daudon, Biospectroscopy, 3, (1997) 347-369.

[4] F. Ana, V. America, S. Roberto, E. Roberto, Rev. Adv. Mater. Sci., 22 (2009) 60-66.
[5] X. Zhu, K. Hou, C. Chen, W. Zhang, H. Sun, G. Zhang, Z. Gao., High Performance Polymers, 27, 2 (2015) 207-216.
[6] S. K. Mishra, R. K. Srivastava, S. G.Prakash, R. S. Yadav, A. C. Panday, Opto−Electronics Rev., 18, 4 (2010) 467-473.
[7] N.V.Joshi, "Photoconductivity", (Marcel Dekker, Inc.), New York, (1990).
[8] B. Sayan , K. Sheo, S. Biswarup, C. Purushottam, Materials Science in Semiconductor Processing, 24 (2014) 200-207.
[9] A. Zainelabdin, S. Zaman, G. Amin, O. Nur, M. Willander, Crystal Growth & Design 10, 7 (2010) 3250-3256.
[10] M. Manickam, V. Ponnuswamy, C. Sankar, R. Suresh, R. Mariappan, J. Chandrasekaran, Int. J. Thin. Fil. Sci. Tec. 5, 3 (2016) 155-161.
[11] K.F.Wadekar, K.R. Nemade, S.A. Waghuley, Research Journal of Chemical, 7, 1 (2017) 53-55.
[12] S. Kerli, Journal of the Korean Physical Society, 71, 7 (2017) 404-407.
[13] J. Hassan, M. Mahdi, A. Ramizy, H. A. Hassan, Z. Hassan, Superlattices and Microstructures, 53 (2013) 31-38.
[14] S. M. Mohammad, Z. Hassan, N. M. Ahmed, N. Al-Hardan, M. Bououdina, Journal of Materials Science, Materials in Electronics 26, 3 (2015) 1322-1331.
[15] Yi, Li Hai-Jin, Zhang Qing Li Yong, Liu Hou-Tong, Chin. Phys., B 22, 5 (2013) 057201-1_057201-6.
[16] I. M. Ali, R. M. Al-Haddad, K. T. Al-Rasoul, IJISET - International Journal of Innovative Science, Engineering & Technology, 1, 10 December (2014) 104-114.
[17] V.R. Shinde, S.B. Mahadik, T.P. Gujar, C.D. Lokhande, Applied Surface Science 252, 20 (2006) 7487-7492.
[18] R.K. Willardson, A.C. Beer, "Semiconductor and Semimetals: Optical Properties of III-V Compounds", Academic Press, New York 1996.
[19] A. Gulino, P. Dapporto, P. Rossi, I. Fragala, Chem. Mater15, 20 (2003) 3748-3752.
[20] S. Thota, A. Kumar, J. Kumar, Mater. Sci. Eng. B164, 1 (2009) 30-37.
[21] A. Green, "Solar Cells", Translated by Y. Hassan, University of Mosul, P.2817, (1989).
[22] J.M. Lui, “Photonic Devices”, Cambridge University Press: Cambridge, (2005).